

Impact of epitaxial structural parameters on two-dimensional hole gas properties in p-GaN/AlGaN/GaN heterostructures

Fuzhou Wen(文福洲), Qianshu Wu(吴千树), Jinwei Zhang(张津玮), Zhuoran Luo(罗卓然), Senyuan Xu(许森源), Hao Jiang(江灏), Yang Liu(刘扬)

Citation: Chin. Phys. B, 2025, 34 (**7**): 077105. DOI: 10.1088/1674-1056/adc97e
http://cpb.iphy.ac.cn; http://iopscience.iop.org/cpb

What follows is a list of articles you may be interested in

Quantum oscillations and nontrivial topology in unfilled skutterudite $IrSb_3$

Yang Yang(杨扬), Xinyao Li(李鑫垚), Feihong Guan(关飞鸿), Majeed Ur Rehman, Wei Ning(宁伟), Xiangde Zhu(朱相德), and Mingliang Tian(田明亮)

Chin. Phys. B, 2025, 34 (**6**): 067103. DOI: 10.1088/1674-1056/adc7f2

Half-metallic ferromagnetic Weyl fermions related to dynamic correlations in the zinc-blende compound VAs

Xianyong Ding(丁献勇), Haoran Wei(魏皓然), Ruixiang Zhu(朱瑞翔), Xiaoliang Xiao(肖晓亮), Xiaozhi Wu(吴小志), and Rui Wang(王锐)

Chin. Phys. B, 2024, 33 (**9**): 097103. DOI: 10.1088/1674-1056/ad5f86

Topological phase transition in compressed van der Waals superlattice heterostructure $BiTeCl/HfTe_2$

Zhilei Li(李志磊), Yinxiang Li(李殷翔), Yiting Wang(王奕婷), Wenzhi Chen(陈文执), and Bin Chen(陈斌)

Chin. Phys. B, 2024, 33 (**8**): 087102. DOI: 10.1088/1674-1056/ad462e

Investigation of helicity-dependent photocurrent of surface states in $(Bi_{0.7}Sb_{0.3})_2Te_3$ nanoplate

Qin Yu(喻钦), Jinling Yu(俞金玲), Yonghai Chen(陈涌海), Yunfeng Lai(赖云锋), Shuying Cheng(程树英), and Ke He(何珂)

Chin. Phys. B, 2024, 33 (**5**): 057101. DOI: 10.1088/1674-1056/ad322c

First-principles study on improvement of two-dimensional hole gas concentration and confinement in AlN/GaN superlattices

Huihui He(何慧卉) and Shenyuan Yang(杨身园)

Chin. Phys. B, 2022, 31 (**1**): 017104. DOI: 10.1088/1674-1056/ac00a0

Impact of epitaxial structural parameters on two-dimensional hole gas properties in p-GaN/AlGaN/GaN heterostructures

Fuzhou Wen(文福洲)[1], Qianshu Wu(吴千树)[1], Jinwei Zhang(张津玮)[1], Zhuoran Luo(罗卓然)[1], Senyuan Xu(许森源)[1], Hao Jiang(江灏)[1], and Yang Liu(刘扬)[1,2,†]

[1] *School of Electronics and Information Technology, Sun Yat-Sen University, Guangzhou* 510006, *China*
[2] *Sun Yat sen University Shenzhen Research Institute, Shenzhen* 518057, *China*

(Received 16 January 2025; revised manuscript received 19 March 2025; accepted manuscript online 7 April 2025)

Research on p-channel field-effect transistors (p-FETs) remains limited, primarily due to the significantly lower conductivity of the two-dimensional hole gas (2DHG) compared to the two-dimensional electron gas (2DEG) in n-channel field-effect transistors (n-FETs), which poses a significant challenge for monolithic integration. In this study, we investigate the impact of epitaxial structure parameters on 2DHG properties in p-GaN/AlGaN/GaN heterostructures through semiconductor technology computer-aided design (TCAD) simulations and theoretical calculations, identifying the conditions necessary to achieve high-density 2DHG. Our simulations demonstrate that increasing the p-GaN thickness leads to two critical thicknesses determined by surface states and acceptor ionization concentration: one corresponds to the onset of 2DHG formation, and the other to its saturation. Lowering the donor surface state energy level and increasing the acceptor ionization concentration promote 2DHG formation and saturation, although the saturated density remains independent of surface states. Additionally, a higher Al composition enhances intrinsic ionization due to stronger polarization effects, thereby increasing the 2DHG sheet density. Consequently, to achieve high-density 2DHG in p-GaN/AlGaN/GaN heterostructures, it is essential to increase the Al composition, ensure that the p-GaN thickness exceeds the critical thickness for 2DHG saturation, and maximize the acceptor ionization concentration. This study elucidates the impact of epitaxial structure parameters on 2DHG properties in p-GaN/AlGaN/GaN heterostructures and provides valuable guidance for the optimization of p-FET designs.

Keywords: p-GaN/AlGaN/GaN heterostructures, 2DHG, surface states, acceptor doping

PACS: 71.55.Eq, 71.23.An, 71.55.–I

DOI: 10.1088/1674-1056/adc97e **CSTR:** 32038.14.CPB.adc97e

1. Introduction

Owing to the strong polarization properties of GaN, the formation of AlGaN/GaN heterojunctions generates high-density positive polarization charges at the interface, inducing the formation of 2DEG. This phenomenon has been extensively utilized in GaN high-electron-mobility transistors (HEMTs).[1–3] The high mobility and low terminal capacitance of the 2DEG[4,5] facilitate high-frequency and high-power-density applications. However, the assembly of discrete GaN devices onto PCB boards introduces additional parasitic inductance.[6,7] Moreover, peripheral circuits are required to drive, control, sense, and protect these core devices.[8] Therefore, monolithic integration processes are urgently needed to fully exploit the potential of GaN electronic devices, reduce parasitic inductance, integrate more functions on-chip, and promote the miniaturization of power conversion systems.[9–13]

In GaN power platforms, logic circuits play a critical role in gate drivers and functional modules. However, the absence of high-performance p-FETs forces reliance on n-channel devices[14] for both GaN power components and peripheral circuits. Although GaN complementary logic (CL) reduces static power consumption compared to direct-coupled FET logic (DCFL),[15–17] the low conductivity of the 2DHG in p-FETs compared to the 2DEG in n-FETs remains a major obstacle for its development.[18,19] Despite the development of some impressive GaN-based complementary metal–oxide–semiconductor devices,[20–22] the performance of p-FETs, particularly their on-state current density, still requires significant improvement.

In the exploration of p-FET channel holes, Nakajima, *et al.*[23] first experimentally demonstrated a high-density 2DHG of 1.1×10^{13} cm^{-2} in a p-GaN/AlGaN heterostructure based on simulation-optimized results. Subsequently, the influence of layer thicknesses above the GaN buffer layer in p-GaN/AlGaN/GaN structures on 2DHG density was further investigated experimentally.[24] To enhance the 2DHG density, strategies such as inserting an AlN layer[25,26] or increasing the Al composition[27] have been proposed. Several studies have explored the origin of 2DHG in p-GaN/AlGaN/GaN structures, with one study[28] proposing that 2DHG arises from the ionization of Mg in the AlGaN barrier layer, where Mg diffuses from the p-GaN layer.

†Corresponding author. E-mail: liuy69@mail.sysu.edu.cn

© 2025 Chinese Physical Society and IOP Publishing Ltd. All rights, including for text and data mining, AI training, and similar technologies, are reserved.

In summary, current research on p-GaN/AlGaN/GaN heterostructures primarily focuses on achieving high-density 2DHG through modifications of structural parameters. However, the impact of these parameter changes on 2DHG density remains incompletely understood, and there is limited research on the sources of 2DHG and its regulation mechanisms under modified structural parameters. In this study, we employ TCAD simulations combined with theoretical analysis to investigate these processes. The research begins with an ideal GaN/AlGaN/GaN heterostructure, incorporating polarization effects, electric fields, and fundamental simulation parameters. Subsequently, by systematically varying the parameters of p-GaN/AlGaN/GaN heterostructures with donor surface states, we explore the sources of 2DHG and its regulation mechanisms, aiming to identify optimal conditions for achieving high-density 2DHG. This work provides valuable insights for optimizing the performance of p-GaN/AlGaN/GaN heterostructures.

2. TCAD simulation settings

In this study, we utilize TCAD simulations to systematically investigate the influence of heterostructure parameters on the 2DHG in p-GaN/AlGaN/GaN structures. First, we introduce the polarization effects, electric fields, and fundamental simulation parameters for GaN/AlGaN/GaN heterostructures. Next, to achieve high-density 2DHG, we examine the effects of structural parameters of the p-GaN layer on 2DHG density, with a focus on the p-GaN layer thickness and acceptor ionization concentration. Additionally, since the energy level of donor surface states in p-GaN may vary depending on the contacting metal, we also investigate the influence of different donor surface state energy levels on 2DHG. Finally, given that the AlGaN layer thickness and Al composition directly influences both 2DHG density and 2DEG formation, we analyze the impact of AlGaN thickness and Al composition on the 2DHG in heterostructures.

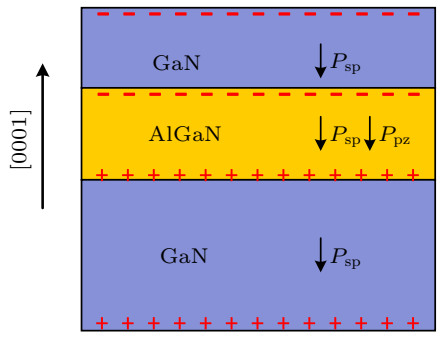


Fig. 1. Polarization charge distribution and interface polarity in Ga-polar GaN/AlGaN/GaN heterostructures.

In this study, the GaN/AlGaN/GaN heterostructures are of Ga-polarity, with the bottom GaN layer in a relaxed state and the AlGaN layer coherently grown on the GaN substrate, resulting in a fully strained AlGaN layer. When GaN is epitaxially grown on the AlGaN layer, the lattice constant remains unaffected by stress, leading to a relaxed top GaN layer. Therefore, the polarization directions in GaN/AlGaN/GaN heterostructures are illustrated in Fig. 1. Negative polarization charges are located at both the top GaN Ga-face and the GaN/AlGaN heterointerface, while positive polarization charges are present at the AlGaN/GaN heterointerface and the bottom GaN N-face.

This study focuses on AlGaN with an Al composition of 30%. The polarization strength of the AlGaN layer depends on its Al content. The spontaneous polarization strength of the AlGaN layer is expressed as

$$P_{\mathrm{sp-AlGaN}} = x_{\mathrm{Al}} P_{\mathrm{sp-AlN}} + (1 - x_{\mathrm{Al}}) P_{\mathrm{sp-GaN}}, \tag{1}$$

where x_{Al} is the Al composition, $P_{\mathrm{sp-AlN}}$ is the spontaneous polarization strength of AlN, and $P_{\mathrm{sp-GaN}}$ is the spontaneous polarization strength of GaN. The AlGaN layer, being fully strained, experiences tensile stress and exhibits piezoelectric polarization. The magnitude of piezoelectric polarization depends on the Al composition and strain. Based on the polarization characteristics of GaN-based semiconductors, the piezoelectric polarization strength is calculated using[4]

$$P_{\mathrm{pz-AlGaN}} = 2 \times \frac{a_{\mathrm{GaN}} - a_{\mathrm{AlGaN}}}{a_{\mathrm{AlGaN}}} \left(e_{13} - e_{33} \frac{C_{13}}{C_{33}} \right), \tag{2}$$

where e_{31} and e_{33} are the piezoelectric coefficients, C_{13} and C_{33} are the stiffness constants, a_{GaN} is the lattice constant of GaN, a_{AlGaN} is the lattice constant of AlGaN, which depends on the Al composition. Here, a_0 denotes the lattice constant common to both AlGaN and GaN when the heterojunction is formed and reaches equilibrium, and a is the actual lattice constant in the horizontal direction of the AlGaN layer and GaN in the initial state, where $a_{\mathrm{Al}_x\mathrm{Ga}_{1-x}\mathrm{N}} = x \cdot a_{\mathrm{AlN}} + (1-x) \cdot a_{\mathrm{GaN}}$. For AlGaN material with an Al composition of 0.3, the total polarization strength is the sum of spontaneous polarization and piezoelectric polarization, resulting in $P_{\mathrm{AlGaN}} = -5.61 \times 10^{-6}$ C/cm^2. For the top and bottom GaN layers, which are fully relaxed, only spontaneous polarization exists, yielding $P_{\mathrm{GaN}} = P_{\mathrm{sp-GaN}} = -2.9 \times 10^{-6}$ C/cm^2, which is consistent with experimental results.[29,30] The parameters related to the simulation are summarized in Table 1.

Table 1. Polarization and material parameters for AlN and GaN at room temperature.

Symbol	Unit	AlN	GaN
P_{sp} (Ref. [31])	C/cm^2	-8.1×10^{-6}	-2.9×10^{-6}
C_{13} (Ref. [30])	Pa	108×10^9	106×10^9
C_{33} (Ref. [30])	Pa	373×10^9	398×10^9
a_0 (Ref. [32])	Å	–	3.189
α (Ref. [32])	Å	3.112	3.189
e_{13} (Ref. [30])	C/cm^2	-6×10^5	-5×10^5
e_{33} (Ref. [30])	C/cm^2	15×10^5	7×10^5

Using Poisson's equation, the polarization electric fields in AlGaN and GaN were calculated as $\epsilon_{\mathrm{AlGaN}} = 3.33$ MV/cm and $\epsilon_{\mathrm{GaN}} = 3.45$ MV/cm, respectively. The results indicate that both AlGaN and GaN exhibit polarization electric fields on the order of MV/cm along the [0001] direction. These electric fields drive carriers along the field direction, causing accumulation at material surfaces or heterojunction interfaces, thereby screening the polarization charges. At the GaN/AlGaN heterojunction interface, the 2DHG is responsible for screening the negative polarization charges. Based on these theoretical calculations, we investigate the impact of epitaxial structural parameters on the 2DHG in p-GaN/AlGaN/GaN heterostructures.

3. Result and discussion

Under the defined simulation conditions, systematic studies were conducted to investigate the impact of p-GaN layer thickness, surface state energy level, acceptor ionization concentration, AlGaN layer thickness and Al composition on the 2DHG in donor surface state-containing p-GaN/AlGaN/GaN heterostructures. Theoretical calculations were simultaneously performed to validate the simulation results, as presented below.

3.1. Impact of p-GaN thickness on 2DHG in heterostructures

In practical GaN growth processes, surface states arise from Ga–O compound formation and Ga-/N-dangling bonds due to surface oxidation.[33] These surface states influence the screening of internal polarization electric fields. Therefore, a high density of donor surface states with energy levels near $E_{\mathrm{c}} - 0.7$ eV is assumed at the p-GaN surface.[34,35] For typical enhancement-mode p-GaN HEMT devices, the acceptor doping concentration is 3×10^{19} cm^{-3}. However, the high activation energy of Mg results in an ionization rate of only $\sim 1\%$ at room temperature. Thus, the effective acceptor ionization concentration is set to 3×10^{17} cm^{-3} to match experimental conditions. The AlGaN layer thickness is fixed at 30 nm with an Al composition of 0.3, and the underlying GaN layer is undoped.

Figure 2(a) shows the band diagrams of heterostructures with donor surface states under varying p-GaN thickness. The conduction band edge (E_{c}) at the Ga-face of the top p-GaN is pinned near the donor surface state energy level. As the p-GaN thickness increases, holes from acceptor ionization are depleted, generating a space charge region that induces band bending. Additionally, figure 2(b) reveals that the pinning position at the p-GaN surface gradually shifts downward within the thickness range of 0 nm–60 nm, indicating a reduced ionization degree of donor surface states.

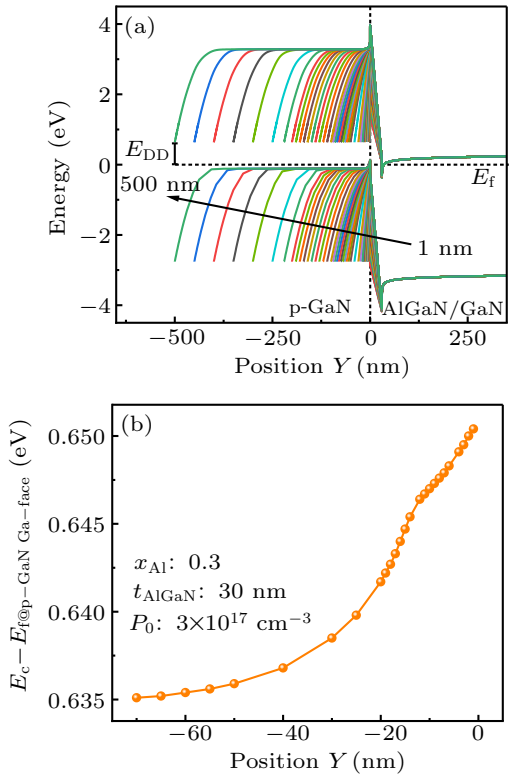


Fig. 2. (a) Band diagrams with increasing p-GaN thickness. (b) The evolution of the pinning position at the Ga-face of the p-GaN layer with varying p-GaN thickness.

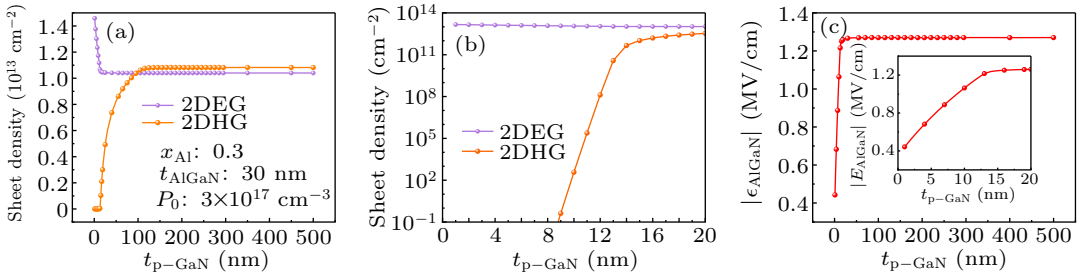


Fig. 3. The 2DEG and 2DHG density modulations by p-GaN thickness: (a) 2DEG and 2DHG sheet density evolutions, (b) critical thickness identification for 2DHG formation (logarithmic scale), (c) AlGaN electric field magnitude ($|\epsilon_{\mathrm{AlGaN}}|$).

Figures 3(a) and 3(b) show the sheet densities of 2DEG and 2DHG as functions of p-GaN thickness. Figure 3(b) demonstrates that a minimum p-GaN thickness is required to form 2DHG at the p-GaN/AlGaN interface. Specifically, the critical thickness for 2DHG formation ($t_{\mathrm{cr-1}}$) is defined as the p-GaN thickness at which the 2DHG sheet density

reaches 1×10^{11} cm^{-2}. For a donor surface state energy level of $E_c - 0.7$ eV and an acceptor ionization concentration of 3×10^{17} cm^{-3}, the corresponding t_{cr-1} is 13.5 nm. Similarly, figure 3(a) indicates that the 2DHG sheet density saturates beyond a critical p-GaN thickness. The critical thickness for saturation (t_{cr-2}) is defined as the thickness at which the 2DHG density deviates from saturation by less than 1%, yielding $t_{cr-2} = 110$ nm under the same conditions.

Figure 4 illustrates the evolution of 2DHG and 2DEG densities with increasing p-GaN thickness, along with the corresponding charge distribution diagrams. Key symbols include: D_{ss} (ionized donor surface state density), $\sigma_{\Pi-AlGaN}$ and $\sigma_{\Pi-GaN}$ (polarization charge densities of AlGaN and GaN), n_{s-2DEG} and p_{s-DHG} (2DEG and 2DHG sheet densities), and Q_{scr} (screening charge density at the N-face).

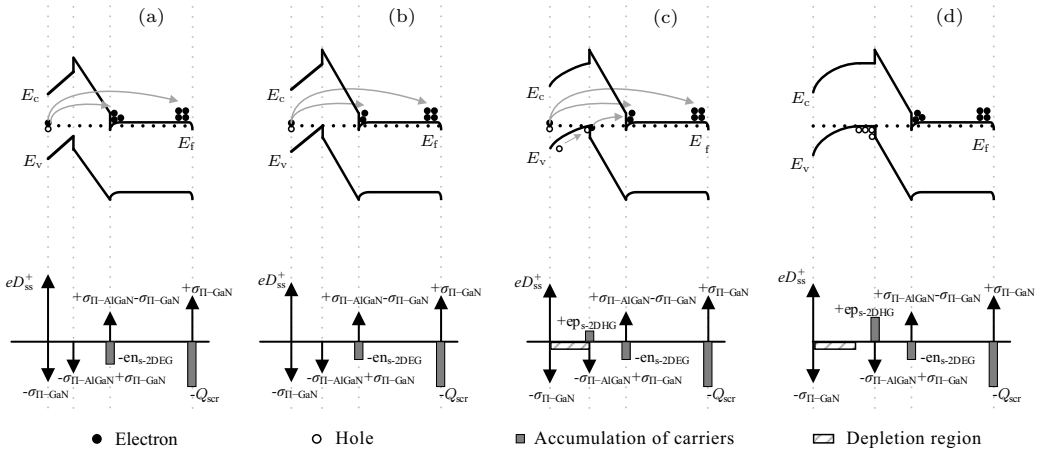


Fig. 4. Charge distributions and screening mechanisms during 2DHG evolution: (a) before the formation of 2DHG formation: complete depletion of holes, (b) formation of 2DHG (t_{cr-1}), (c) progressive 2DHG density increase, (d) saturation of 2DHG and 2DEG densities (t_{cr-2}).

As shown in Fig. 4(a), for thin p-GaN layers ($t_{p-GaN} \leq t_{cr-1}$), holes generated by acceptor ionization near the Ga-face are completely depleted by electrons from donor surface states. This results in downward bending of the corresponding energy band, while the conduction band edge at the Ga-face is pinned near the donor surface state energy level. The large number of electrons generated by donor ionization screen the positive polarization charges at the bottom N-face, with the excess electrons forming a high-density 2DEG.

Simultaneously, the higher density of ionized donor surface states compared to negative polarization charges results in a net positive surface charge, reversing the electric field in the p-GaN layer. As the p-GaN thickness increases, reduced ionization of donor surface states enhances the AlGaN layer's electric field (Fig. 3(c)), pushing the E_v at the p-GaN/AlGaN interface closer to the E_f. The onset of 2DHG formation occurs at t_{cr-1}, as shown in Fig. 4(b), with the AlGaN electric field remaining constant.

Figure 4(c) shows that for $t_{cr-1} < t_{p-GaN} < t_{cr-2}$, both acceptor ionization in the p-GaN layer and intrinsic ionization near the p-GaN/AlGaN interface increase. The holes generated by ionization drift to the heterojunction interface under the reversed electric field of the p-GaN, leading to a continuous increase in the 2DHG sheet density. Concurrently, reduced ionization of donor surface states and enhanced intrinsic ionization stabilize the 2DEG density.

Figure 4(d) demonstrates that for $t_{p-GaN} \geq t_{cr-2}$, holes near the p-GaN surface drift to the p-GaN/AlGaN interface, forming a space charge region. This results in downward band bending in the corresponding region. The closer to AlGaN layer, the energy band of p-GaN becomes flatter, and the critical point occurs at t_{cr-2}. At $t_{p-GaN} = t_{cr-2}$, electrostatic equilibrium is achieved between the negative polarization charge at the p-GaN Ga-face, positively charged ionized donor surface states, and negatively charged ionized acceptor impurities. Consequently, further increases in p-GaN thickness do not enhance the 2DHG sheet density.

3.2. Impact of p-GaN surface state energy level and acceptor ionization concentration on 2DHG in heterostructures

Following the analysis of p-GaN layer thickness effects on 2DHG in p-GaN/AlGaN/GaN heterostructures, this section investigates the influence of p-GaN surface state energy level and acceptor ionization concentration on 2DHG.

First, the impact of the p-GaN surface state energy level on 2DHG was examined by varying the donor surface state energy level from $E_c - 1.1$ eV to $E_c - 0.3$ eV (i.e., approaching E_c) in TCAD simulations. With the p-GaN thickness fixed at 300 nm (exceeding t_{cr-2}, ensuring 2DHG saturation), the energy band distributions for different surface state energy levels are shown in Fig. 5(a). Figures 5(b) and 5(c) show the variation of 2DHG sheet density with p-GaN thickness, reveal that increasing the surface state energy level raises both critical thicknesses: t_{cr-1} increases from 11.5 nm to 15.3 nm, and t_{cr-2} increases from 103.4 nm to 118 nm. This indicates that lower

surface state energy levels promote higher 2DHG sheet densities. Additionally, when $t_{\mathrm{p-GaN}} > t_{\mathrm{cr-2}}$, variations in surface state energy level negligibly affect the saturated 2DHG density. However, changes in Al composition or interface defects can alter the interfacial polarization strength, thereby influencing the 2DHG density. For instance, a higher Al composition enhances intrinsic ionization, increasing the 2DHG density independently of surface states (see the inset of Fig. 5(b)).

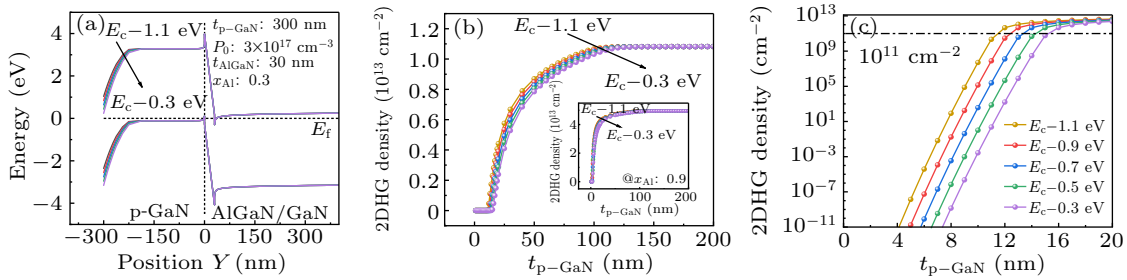


Fig. 5. Impact of surface state energy levels on 2DHG formation: (a) band diagrams for E_{DD} ranging from $E_c-1.1$ eV to $E_c-0.3$ eV, (b) global trends of 2DHG density at $x_{\mathrm{Al}}=0.3$. The inset shows the trends at $x_{\mathrm{Al}}=0.9$, (c) critical thickness $t_{\mathrm{cr-1}}$ dependence (logarithmic scale).

Furthermore, the impact of acceptor ionization concentration on 2DHG was studied by varying the p-GaN acceptor ionization concentration from 0 to 1×10^{18} cm^{-3} in the TCAD simulations. Figure 6(a) shows the energy band distribution for different acceptor ionization concentrations at a fixed p-GaN thickness of 300 nm. Figures 6(b) and 6(c) depict the variation of 2DHG sheet density with increasing p-GaN thickness. As shown in Figs. 6(b) and 6(c), increasing the acceptor ionization concentration slightly reduces the critical thickness $t_{\mathrm{cr-1}}$. Notably, compared to the case without acceptor doping (where the 2DHG density remains low and difficult to saturate), elevating the acceptor ionization concentration from 1×10^{17} cm^{-3} to 1×10^{18} cm^{-3} significantly decreases $t_{\mathrm{cr-2}}$ from 167.3 nm to 71.5 nm, accompanied by a marked increase in the saturated 2DHG density. These results underscore the critical role of acceptor ionization concentration in 2DHG formation.

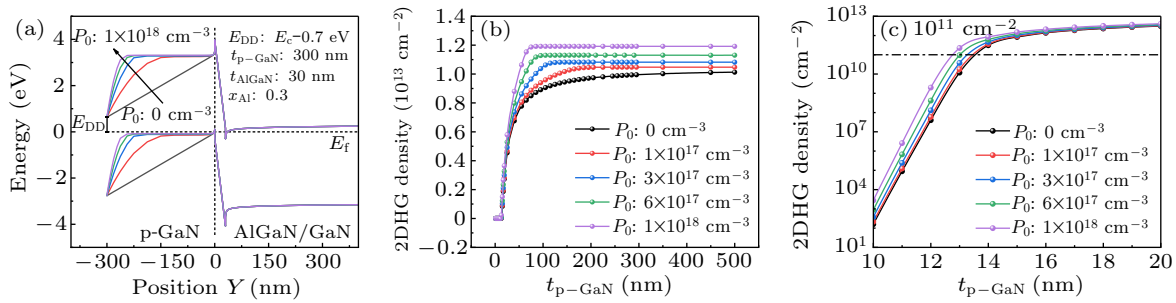


Fig. 6. Acceptor concentration dependence of 2DHG saturation: (a) band diagrams for P_0 from 0 to 1×10^{18} cm^{-3}, (b) saturation behavior of 2DHG density, (c) critical thickness $t_{\mathrm{cr-2}}$ reduction trend (logarithmic scale).

To validate the simulated critical thicknesses ($t_{\mathrm{cr-1}}$ and $t_{\mathrm{cr-2}}$), theoretical calculations were performed.

For $t_{\mathrm{cr-1}}$, due to its small thickness, the electric field in the p-GaN layer can be assumed constant, with approximately parallel energy bands. Thus, $t_{\mathrm{cr-1}}$ is derived as

$$t_{\mathrm{cr-1}} = \frac{E_{\mathrm{g\text{-}GaN}} - E_{\mathrm{DD}}}{e\epsilon_{\mathrm{p\text{-}GaN}}}, \tag{3}$$

where $E_{\mathrm{g\text{-}GaN}}$ is the bandgap energy of GaN, E_{DD} is the surface state energy level, which is 0.7 eV in this case, e is the electron charge, and $\epsilon_{\mathrm{p\text{-}GaN}}$ is the electric field strength in the p-GaN layer, which can be calculated from the net charge density at the p-GaN surface and the p-GaN/AlGaN interface. Neglecting electric field variations in the p-GaN layer, the AlGaN layer's electric field ($\epsilon_{\mathrm{AlGaN}}$) is given by

$$\epsilon_{\mathrm{AlGaN}} = \frac{E_{\mathrm{g\text{-}AlGaN}}}{et_{\mathrm{AlGaN}}}. \tag{4}$$

Here, $E_{\mathrm{g\text{-}AlGaN}}$ represents the bandgap energy of AlGaN, and t_{AlGaN} denotes the thickness of the AlGaN layer. When $t_{\mathrm{p\text{-}GaN}}$ reaches $t_{\mathrm{cr-1}}$, both interfaces of the AlGaN layer become pinned, rendering $\epsilon_{\mathrm{AlGaN}}$ independent of the presence of the p-GaN layer. For a 30-nm AlGaN layer, $\epsilon_{\mathrm{AlGaN}}$ is calculated as 1.34 MV/cm. Using Poisson's equation, the net negative charge density at the p-GaN/AlGaN interface is calculated as 7×10^{12} cm^2.

At the p-GaN surface, ionized electrons completely screen the positive polarization charge at the bottom GaN N-face and partially screen the positive polarization charge at the AlGaN/GaN interface. Consequently, the p-GaN surface retains a net remaining positive charge density of 1.05×10^{13} cm^2, which matches the partially screened positive polarization charge density at the AlGaN/GaN interface. As the underlying GaN electric field is fully screened, $\epsilon_{\mathrm{p\text{-}GaN}}$

is determined by the net charges at the p-GaN surface and the p-GaN/AlGaN interface. Using Poisson's equation, $\epsilon_{\text{p-GaN}}$ is calculated as 1.67 MV/cm. Substituting it into Eq. (3), $t_{\text{cr}-1}$ is obtained.

Figure 7(a) compares the theoretical and simulated values of $t_{\text{cr}-1}$ as a function of the p-GaN surface state energy level. The figure reveals minor discrepancies between the theoretical and simulated results. These discrepancies primarily arise from neglecting the contribution of holes from p-GaN ionization in the theoretical analysis. The theoretical analysis assumes parallel energy bands for $t_{\text{p-GaN}} < t_{\text{cr}-1}$, leading to an overestimation of $t_{\text{cr}-1}$ compared to the simulation results.

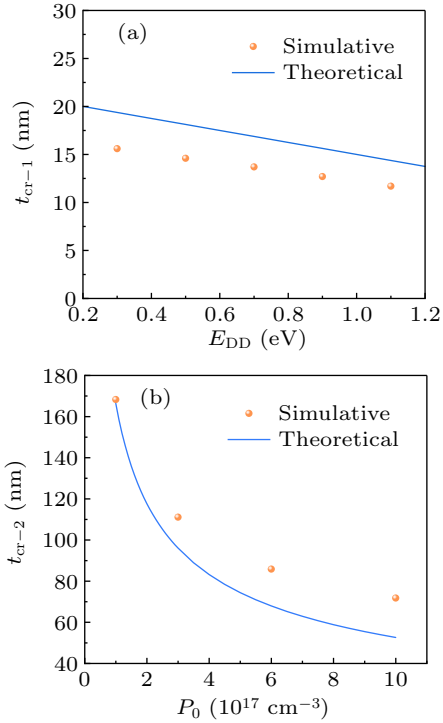


Fig. 7. Validation of critical thickness models: (a) surface state energy dependence of $t_{\text{cr}-1}$, (b) acceptor concentration dependence of $t_{\text{cr}-2}$.

The critical thickness $t_{\text{cr}-2}$, corresponding to 2DHG saturation, is analogous to the depletion region width of the p-GaN and is expressed as

$$t_{\text{cr}-2} = \sqrt{\frac{2\varepsilon V_{\text{bi}}}{eN_{\text{A}}}}, \tag{5}$$

where ε is the dielectric constant of GaN, V_{bi} is the built-in potential, and N_{A} is the acceptor ionization concentration. The built-in potential V_{bi} is given by

$$V_{\text{bi}} = E_{\text{g-GaN}} - E_{\text{DD}} - (E_{\text{f}} - E_{\text{v}}), \tag{6}$$

where E_{f} is the Fermi level, E_{v} is the valence band edge, and $E_{\text{f}} - E_{\text{v}} = -kT\ln(N_{\text{A}}/N_{\text{V}})$, with N_{V} being the valence band effective density of states for GaN. Substituting Eq. (6) into Eq. (5), $t_{\text{cr}-2}$ can be expressed as

$$t_{\text{cr}-2} = \sqrt{\frac{2\varepsilon\left[E_{\text{g-GaN}} - E_{\text{DD}} + k_0 T\ln\left(N_{\text{A}}/N_{\text{V}}\right)\right]}{eN_{\text{A}}}}. \tag{7}$$

Based on the above analysis, the critical thickness $t_{\text{cr}-2}$ at room temperature can be calculated. Figure 7(b) presents the theoretical and simulation values of $t_{\text{cr}-2}$ for different p-GaN acceptor ionization concentrations. The figure demonstrates excellent agreement between the theoretical and simulated results.

3.3. Impact of AlGaN thickness and Al composition on the 2DHG in heterostructures

Finally, We note that the AlGaN layer thickness (t_{AlGaN}) and Al composition (x_{Al}) critically governs both the 2DHG sheet density and the formation of the 2DEG, necessitating further investigation into their underlying mechanisms. Previous results indicate that when $t_{\text{p-GaN}} > t_{\text{cr}-2}$, both 2DHG and 2DEG sheet densities stabilize. Therefore, in the subsequent analysis, the p-GaN thickness is fixed at 300 nm (exceeding $t_{\text{cr}-2}$), with the surface state energy level set to $E_{\text{c}} - 0.7$ eV and acceptor ionization concentration fixed at 3×10^{17} cm^{-3}, to explore the impact of AlGaN layer parameters on 2DHG.

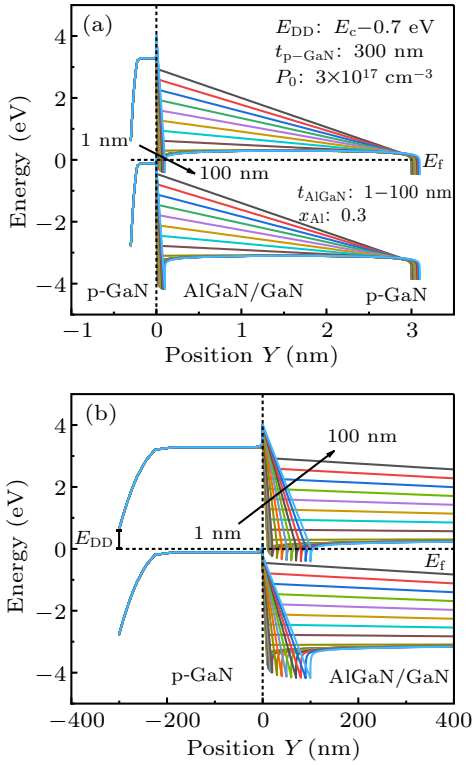


Fig. 8. Band structure evolution with AlGaN thickness: (a) global trends, (b) interface band pinning at the AlGaN/GaN heterojunction.

First, the impact of AlGaN layer thickness on 2DHG is investigated. At the x_{Al} of 0.3, the band diagrams for different AlGaN thicknesses are shown in Fig. 8. Figures 9(a) and 9(b) illustrate the evolution of 2DHG and 2DEG sheet densities with increasing t_{AlGaN}. As shown in Fig. 9(b), 2DEG formation at the AlGaN/GaN interface requires a minimum AlGaN thickness ($t_{\text{cr-AlGaN}}$), calculated as $t_{\text{cr-AlGaN}} = E_{\text{g-AlGaN}}/(e\epsilon_{\text{AlGaN}})$, yielding $t_{\text{cr-AlGaN}} = 11$ nm. At this point, the 2DEG sheet density reaches 10^{11} cm^{-2}. For $t_{\text{AlGaN}} <$

$t_{\text{cr-AlGaN}}$, the E_c at the AlGaN/GaN interface is far from the E_f, suppressing intrinsic ionization and depleting the 2DEG. Meanwhile, acceptor ionization in p-GaN maintains a constant 2DHG sheet density of 1.1×10^{12} cm^{-2}. For $t_{\text{AlGaN}} > t_{\text{cr-AlGaN}}$, E_c at the AlGaN/GaN interface aligns with and pins to E_f, enhancing intrinsic ionization and progressively increasing both 2DHG and 2DEG densities. This trend is further supported by the AlGaN layer's electric field variation (Fig. 9(c)).

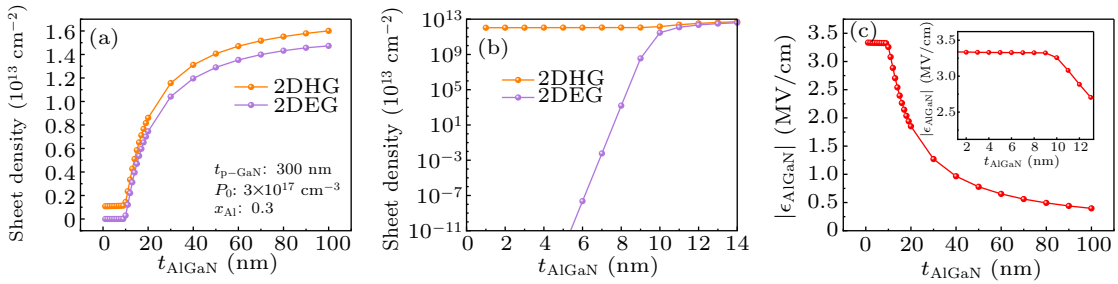


Fig. 9. The 2DHG and 2DEG density modulations by AlGaN thickness: (a) global trends of carrier density evolution, (b) critical AlGaN thickness identification (logarithmic scale), (c) AlGaN electric field magnitude ($|\epsilon_{\text{AlGaN}}|$).

Notably, when $t_{\text{AlGaN}} > t_{\text{cr-AlGaN}}$, intrinsic ionization drives the 2DHG and 2DEG densities to exceed 10^{13} cm^{-2}, with less than 10% of holes contributed by p-GaN ionization. This indicates that acceptor ionization in p-GaN has limited capacity to enhance 2DHG density, while polarization-induced intrinsic ionization dominates at the heterojunction.

Next, the impact of Al composition on 2DHG is investigated by varying the x_{Al} from 0.1 to 0.9. The band diagrams for different x_{Al} at the AlGaN layer thickness of 30 nm are shown in Fig. 10(a). It can be observed that increasing the x_{Al} leads to a more pronounced band bending in the AlGaN layer, indicating a stronger polarization-induced electric field (refer to Eq. (1)). Consequently, the enhanced polarization field promotes stronger intrinsic ionization, resulting in a continuous increase in 2DHG and 2DEG densities (Fig. 10(b)). Additionally, figure 10(b) reveals that lower x_{Al} requires a larger critical AlGaN thickness ($t_{\text{cr-AlGaN}}$) for 2DEG formation. This critical thickness corresponds to the point where the E_c at the AlGaN/GaN interface contacts the E_f. When $t_{\text{AlGaN}} > t_{\text{cr-AlGaN}}$, intrinsic ionization causes the 2DHG and 2DEG sheet densities to rise simultaneously. These trends are further supported by the variation in the electric field within the AlGaN layer, as shown in Fig. 10(c). The inflection point in the AlGaN electric field corresponds to $t_{\text{cr-AlGaN}}$, which decreases from 30 nm to 3 nm as the x_{Al} increases from 0.1 to 0.9.

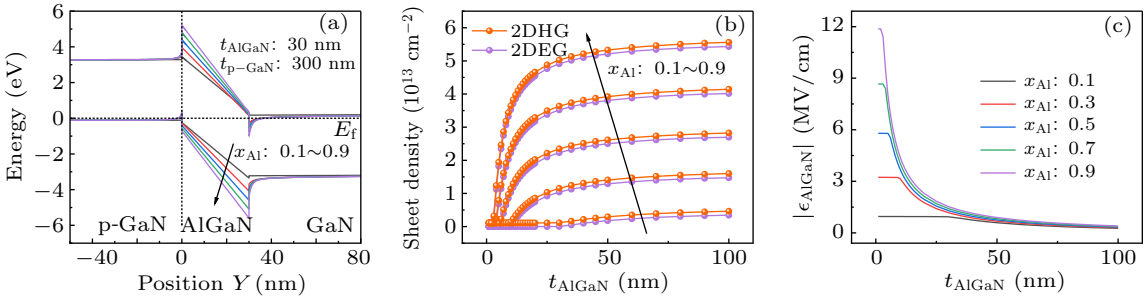


Fig. 10. The 2DHG and 2DEG density modulations by Al composition: (a) band diagrams for x_{Al} from 0.1 to 0.9, (b) 2DEG and 2DHG sheet densities versus t_{AlGaN}, (c) $|\epsilon_{\text{AlGaN}}|$ versus t_{AlGaN}.

In concise, a higher Al composition enhances the polarization-induced electric field in the AlGaN layer, thereby driving intrinsic ionization to generate higher densities of 2DHG and 2DEG.

4. Conclusion

Through systematic TCAD simulations and theoretical analysis, we investigated the impact of epitaxial structure parameters on the 2DHG properties in p-GaN/AlGaN/GaN heterostructures, revealing the conditions necessary for achieving high-density 2DHG.

We demonstrate that two critical p-GaN thicknesses govern 2DHG behavior: which correspond to the onset and saturation of 2DHG, respectively. These two critical thicknesses emerge from the combined effects of donor surface state-induced band pinning (depleting acceptor-generated holes) and electrostatic equilibrium between polarization charges, ionized surface states, and acceptor impurities. Lowering the donor surface state energy level (away from the E_c) and enhancing acceptor ionization concentration collectively reduce both critical thicknesses, accelerating 2DHG formation and saturation, although the saturated density remains independent of surface states. Additionally, a higher Al composition enhances intrinsic ionization due to stronger polarization effects,

thereby increasing the 2DHG density.

Consequently, to achieve high-density 2DHG in heterostructures, it is essential to increase the Al composition, ensure that the p-GaN thickness exceeds the critical thickness for 2DHG saturation, and maximize the acceptor ionization concentration. This study elucidates the impact of epitaxial structure parameters on 2DHG properties in p-GaN/AlGaN/GaN heterostructures, providing valuable insights for the optimization and design of p-FET structures.

Acknowledgements

Project supported by the National Key Research and Development Program of China (Grant No. 2022YFB3604203), the Key Research and Development Program of Guangdong Province, China (Grant No. 2024B0101060002), and the Key Research and Development Program of Shenzhen City, China (Grant No. JCYJ20241202130036043).

References

[1] Haziq M, Falina S, Manaf A A, Kawarada H and Syamsul M 2022 *Micromachines* **13** 2133
[2] Islam N, Mohamed M F P, Khan M F A J, Falina S, Kawarada H and Syamsul M 2022 *Crystals* **12** 1581
[3] He J, Cheng W C, Wang Q, Cheng K, Yu H and Chai Y 2021 *Adv. Electronic Materials* **7** 2001045
[4] Ambacher O, Smart J, Shealy J R, Weimann N G, Chu K, Murphy M, Schaff W J, Eastman L F, Dimitrov R, Wittmer L, Stutzmann M, Rieger W and Hilsenbeck J 1999 *J. Appl. Phys.* **85** 3222
[5] Chen K J, Häberlen O, Lidow A, lin Tsai C, Ueda T, Uemoto Y and Wu Y 2017 *IEEE Trans. Electron Dev.* **64** 779
[6] Huque M A, Islam S K, Tolbert L M and Blalock B J 2012 *IEEE Trans. Power Electron.* **27** 4153
[7] Cui M, Bu Q, Cai Y, Sun R, Liu W, Wen H, Lam S, Liang Y C, Mitrovic I Z and Taylor S 2019 *Jpn. J. Appl. Phys.* **58** 056505
[8] Emon A I, Mirza A B, Kaplun J, Vala S S and Luo F 2022 *IEEE J. Emerg. Select. Top. Power Electron.* **11** 2707
[9] Trescases O, Murray S, Jiang W and Zaman M 2020 *IEEE International Electron Devices Meeting (IEDM)*, December 12–18, Electr Network, p. 27.4.1
[10] Basler M, Reiner R, Moench S, Benkhelifa F, Döring P, Waltereit P, Quay R and Ambacher O 2021 *IEEE Access* **9** 163122
[11] Wei J, Zheng Z, Tang G, Xu H, Lyu G, Zhang L, Chen J, Hua M, Feng S and Chen T 2023 *IEEE Trans. Electron Dev.* **71** 1365
[12] Wei J, Tang G, Xie R and Chen K J 2020 *Jpn. J. Appl. Phys.* **59** SG0801
[13] Sun R, Liang Y C, Yeo Y C, Zhao C, Chen W and Zhang B 2019 *IEEE J. Emerg. Selec. Top. Power Electron.* **8** 31
[14] Tang G, Kwan A M, Wong R K, Lei J, Su R, Yao F, Lin Y, Yu J, Tsai T and Tuan H 2017 *IEEE Electron Dev. Lett.* **38** 1282
[15] Amano H, Baines Y, Beam E, Borga M, Bouchet T, Chalker P R, Charles M, Chen K J, Chowdhury N and Chu R 2018 *J. Phys. D: Appl. Phys.* **51** 163001
[16] Wong K Y R, Kwan M H, Yao F W, Tsai M W, Lin Y S, Chang Y C, Chen P C, Su R Y, Yu J L, Yang F J, Lansbergen G P, Hsiung C W, Lai Y A, Chiu K L, Chen C F, Lin M C, Wu H Y, Chiang C H, Liu S D, Chiu H C, Liu P C, Chen C M, Yu C Y, Tsai C S, Wu C B, Lin B, Chang M H, You J S, Wang S P, Chen L C, Liao Y Y, Tsai L Y, Tsai T, Tuan H C and Kalnitsky A 2015 *IEEE International Electron Devices Meeting (IEDM)*, December 07–09, Washington, DC, p. 9.5.1
[17] Van Hove M, Boulay S, Bahl S R, Stoffels S, Kang X, Wellekens D, Geens K, Delabie A and Decoutere S 2012 *IEEE Electron Dev. Lett.* **33** 667
[18] Bader S J, Lee H, Chaudhuri R, Huang S, Hickman A, Molnar A, Xing H G, Jena D, Then H W and Chowdhury N 2020 *IEEE Trans. Electron Dev.* **67** 4010
[19] Peralagu U, Alian A, Putcha V, Khaled A, Rodriguez R, Sibaja-Hernandez A, Chang S, Simoen E, Zhao S E, De Jaeger B, Fleetwood D M, Wambacq P, Zhao M, Parvais B, Waldron N and Collaert N 2019 *IEEE International Electron Devices Meeting (IEDM)*, December 09–11, San Francisco, CA, p. 17.2.1
[20] Zheng Z, Zhang L, Song W, Feng S, Xu H, Sun J, Yang S, Chen T, Wei J and Chen K 2021 *Nat. Electron.* **4** 595
[21] Hahn H, Reuters B, Kotzea S, Lükens G, Geipel S, Kalisch H and Vescan A 2014 *72nd Annual Device Research Conference (DRC)*, June 22–25, Univ Calif, Santa Barbara, CA, p. 259
[22] Chu R, Cao Y, Chen M, Li R and Zehnder D 2016 *IEEE Electron Dev. Lett.* **37** 269
[23] Nakajima A, Sumida Y, Dhyani M H, Kawai H and Narayanan E M S 2010 *Appl. Phys. Express* **3** 121004
[24] Nakajima A, Liu P, Ogura M, Makino T, Kakushima K, Nishizawa S I, Ohashi H, Yamasaki S and Iwai H 2014 *J. Appl. Phys.* **115** 153707
[25] Wang Y, Huang S, Jiang Q, Wang X, Ji Z, Fan J, Yin H, Wei K, Liu X, Sun Q and Chen K J 2023 *Appl. Phys. Lett.* **123** 262107
[26] He H and Yang S 2022 *Chin. Phys. B* **31** 017104
[27] Shao P, Fan X, Li S, Chen S, Zhou H, Liu H, Guo H, Xu W, Tao T, Xie Z, Lu H, Wang K, Liu B, Chen D, Zheng Y and Zhang R 2023 *Appl. Phys. Lett.* **122** 142102
[28] Ng Y H, Zheng Z, Zhang L, Liu R, Chen T, Feng S, Shao Q and Chen K J 2023 *Appl. Phys. Lett.* **123** 142106
[29] Lähnemann J, Brandt O, Jahn U, Pfüller C, Roder C, Dogan P, Grosse F, Belabbes A, Bechstedt F, Trampert A and Geelhaar L 2012 *Phys. Rev. B* **86** 081302
[30] Bernardini F, Fiorentini V and Vanderbilt D 1997 *Phys. Rev. B* **56** 10024
[31] Yan W S, Zhang R, Xiu X Q, Xie Z L, Han P, Jiang R L, Gu S L, Shi Y and Zheng Y D 2007 *Appl. Phys. Lett.* **90** 212102
[32] Rumyantsev S L, Shur M S and Levinshtein M E 2004 *International Journal of High Speed Electronics and Systems* **14** 1
[33] Shalish I, Shapira Y, Burstein L and Salzman J 2001 *J. Appl. Phys.* **89** 390
[34] Chen J, Huang W, Qu H, Zhang Y, Zhou J, Chen B and Zou X 2022 *Appl. Phys. Lett.* **120** 212105
[35] Sang L, Ren B, Nabatame T, Sumiya M and Liao M 2021 *J. Alloys Compd.* **853** 157356 (in Chinese)